Bioinspired Obstacle Avoidance Algorithms for Robot Swarms

Jérôme Guzzi, Alessandro Giusti,
Luca M. Gambardella, and Gianni A. Di Caro

Dalle Molle Institute for Artificial Intelligence (IDSIA), Manno-Lugano, Switzerland
{jerome,alessandrog,luca,gianni}@idsia.ch,
WWW home page: http://www.idsia.ch/~gianni/SwarmRobotics

Abstract. Recent work in socio-biological sciences have introduced simple heuristics that accurately explain the behavior of pedestrians navigating in an environment while avoiding mutual collisions. We have adapted and implemented such heuristics for distributed obstacle avoidance in robot swarms, with the goal of obtaining human-like navigation behaviors which would be perceived as friendly by humans sharing the same spaces. In this context, we study the effects of using different sensing modalities and robot types, and introduce robot's emotional states, which allows us to modulate system's group behavior. Experimental results are provided for both real and simulated robots. The extensive quantitative simulations show the macroscopic behavior of the system in various scenarios, where we observe emergent collective behaviors – some of which are similar to those observed in human crowds.

Key words: Dynamic obstacle avoidance, human-friendly navigation, mobile robots, emerging macroscopic behaviors, emotions

1 Introduction

Which mechanisms do pedestrians use in order to navigate around moving obstacles in a dynamic environment? Social anthropologists and researchers concerned with simulating crowd behavior have proposed several different models for explaining human obstacle avoidance behaviors. Among these, Moussaid et al. [1] have recently proposed a simple heuristic (inspired by specific functions of the human eye and the brain) which is able to accurately predict observed trajectories, as well as macroscopic behaviors, observed in crowds – such as the spontaneous formation of ordered lines of opposite flow in corridors.

We propose to adopt the same obstacle avoidance heuristic in robot swarms, and present a working implementation on real robots and simulations. If robots follow the same mobility criteria as pedestrians, their trajectories will be *predictable* and *legible* to humans sharing the same spaces. The resulting behaviors would then be perceived as *friendly* and *acceptable*, ultimately enabling efficient sharing of spaces among humans and robot swarms, which is the long-term goal of our research.

Unlike humans, which can be modeled as agents with practically homogeneous dynamic and sensing abilities, robots are characterized by a much larger variability in terms of operational capabilities. For example, different kinds of robots may move at quite different speeds, or may be able to sense other agents based on different fields of view and accuracy. Given these core differences, in which conditions can we still observe human-like macroscopic behaviors? Can we introduce simple variations to the core heuristic to promote the emergence of novel collective behaviors useful in typical swarm robotic scenarios? This paper presents our first results in answering such questions by means of quantitative simulations of large robot swarms. In turn, simulation results are validated with an implementation of the same algorithms on real robots, the *foot-bots* [2].

The rest of the paper is organized as follows. Section 2 relates our work to other obstacle-avoidance algorithms in robotics and to recent research in crowd modeling. In Section 3 we briefly describe the core obstacle-avoidance heuristic, first proposed in [1], then detail our implementation in robotics and describe its parameters. Moreover, we discuss simple variations aimed at promoting new meaningful behaviors in robot swarms, such as the autonomous, emotion-driven formation of homogeneous groups of robots with similar attitudes and characteristics. Section 4 shows the details of our implementation for real robots and our simulation environment, which in used in Section 5 to run a number of quantitative experiments considering different scenarios.

2 Related Work

The problem of dynamic obstacle avoidance is widely studied both in robotics and social sciences. Our works builds upon results in both fields.

In robotics, the most common approach is based on the concept of *velocity obstacle* [3], also known as *collision cone* or *forbidden velocity map*, meaning the sets of velocities that will lead a robot to collision: choosing a velocity outside such set ensures that no collision will occur. Different variations of these ideas have been presented to improve the prediction accuracy of other agents' trajectories, to add recursion and account for sensing errors in a probabilistic framework [4], and to ensure smooth trajectories by sharing the responsibility to avoid a collision with other agents (*reciprocal velocity obstacle* [5]). Applications to very crowded scenarios also introduce asymmetries in the obstacle velocity construction [6], requiring to enforce conventions to allow smooth and deterministic interactions between agents. The velocity-obstacle model was also successfully applied to explain certain characteristics of pedestrian behavior [7].

All the mentioned works basically build on a mechanicistic and artificial approach to navigation, which is designed to ensure safety, and is adapted to produce smooth trajectories. On the contrary, our work stems from a cognitive heuristic [1] modeling human behavior – which produces paths with good efficiency, smoothness, and legibility – to which we add some modifications to also ensure safety (a primary objective in robotics). This paper represents the first

implementation of this heuristic to robotics. Implementation-wise, such a heuristic allows us to decouple the computation of speed and desired heading for the navigating agent. This leads to a simpler implementation than velocity-obstacle approaches, which requires a search over the two-dimensional velocity space.

Animals are able to visually control locomotion through optical flow [8], which provides a direct estimation of the current *time to contact* τ with a moving obstacle. For instance, humans use optical flow to control the speed of walking [9] and to perceive upcoming collisions [10], both from internal and external point of views, drivers use it to control braking ($\dot{\tau}$ strategy) and to adjust for a safe distance from the preceding car [11]. This sensing information is fed into a spatial-temporal integration and *temporal prediction* cognitive layer [12] for collision prediction and, in general, is incorporated into higher level cognitive processes. Through neuromodulation [13] internal brain states, like those related to emotions, modulate the sensing and behavioral process. In robotics, this provides a framework to improve learning, flexibility, robustness and control the emergence of cooperative behaviors [14, 15]. Following these observations, we also include the use of emotional states as modulators of navigational behaviors.

Mutual avoidance and sharing of space in human groups has been extensively studied in sociological research for the prediction of the behavior of crowds, among other topics that have been considered. The original models are based on the study of *proxemics* [16], which formalizes the concept of *personal* and *social* space, where pedestrian behavior based on *social forces* [17] enforces people to keep a minimum distance from neighbors whenever possible. Such modeling approach was successfully used for crowd simulation and also inspired several human tracking and avoidance models in robotics. The density dependence of the speed of a flow of people along a street can be explained by the *net-time headway* mechanism [18], according to which each pedestrian keeps a constant τ time away from the surrounding pedestrians to avoid collisions and stops walking if this would imply a low speed. Moussaid et al. [1, 19] recently incorporated this rule in a new model of pedestrian navigation based on a simple heuristic, which we build upon and extend it for use in robot swarms. Among other topics the authors also addressed the bidirectional pedestrian flow scenario that is relevant for virtual crowds simulation and for the study of emerging behaviors like lines formation [20]. We also consider similar situations.

3 The Models for Human and Robot Navigation

We first discuss the heuristics explaining human behavior for obstacle-avoidance as introduced by [1] (Section 3.1), then present our adaptation to robotics (Section 3.2) and an extension for including artificial emotional states, which depend on the presence of close by robots with similar attitudes and characteristics, and is used to modulate group behavior (Section 3.3).

3.1 Human Behavioral Model

Given a 2D reference frame F, a moving agent directed to a target point $\vec{O}$ is characterized by an optimal (open space) moving speed v_{opt} and a horizontal field of view 2ϕ (in radians). In the reference frame F, $\vec{x}(t)$ and $\vec{v}(t)$ are agent's position and velocity vectors at time t, and $\alpha(t)$ is agent's heading, (i.e., the direction it is facing with respect to F's horizontal axis). We assume that agent's ground occupancy is approximated by a circle of known radius r.

To direct its movements, the agent makes use of a cognitive function $f(\alpha),\ \alpha \in [\alpha(t) - \phi,\ \alpha(t) + \phi]$, based on visual information, that maps each heading α within its field of view to the distance that the agent can travel in $\alpha's$ direction before colliding with any visible obstacle when moving at speed v_{opt}. The distance is bounded by a maximum horizon H. With $s(\alpha)$ we denote the 2D segment connecting $\vec{x}$ with the point at distance $f(\alpha)$ along the direction α (i.e., the point of first collision for heading α). When computing $f(\alpha)$, all obstacles are assumed to keep their current heading and speed, thus moving according to a uniform linear motion.

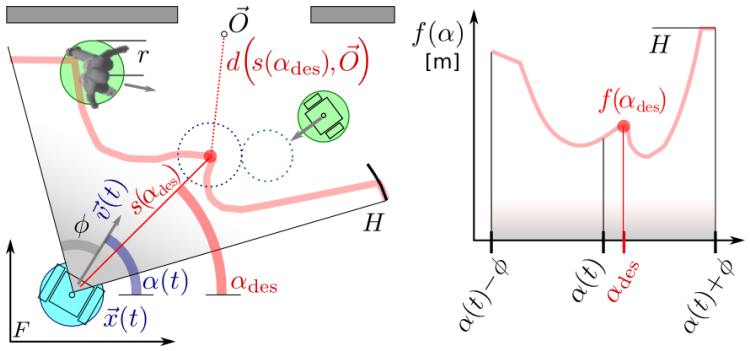

Fig. 1. Illustration of variables and functions for the human navigation model.

Given the above notations, the agent walking behavior can be explained by the following simple heuristic rules.

First, the agent determines its desired heading $\alpha_{\text{des}}(t)$ as the direction allowing the most direct path to destination point $\vec{O}$, taking into account the presence of obstacles:

$$\alpha_{\text{des}}(t) = \text{argmin}_{\alpha}\, d\left(s\left(\alpha\right), \vec{O}\right)\ , \tag{1}$$

where $d(\cdots)$ denotes the minimal distance between a line segment and a point.

The desired velocity vector $\vec{v}_{\text{des}}(t)$ is then determined. Its direction is defined by the heading $\alpha_{\text{des}}(t)$, and its modulus $v_{\text{des}}(t)$ is set to allow stopping in a fixed time τ_1 within the free distance $D(\alpha_{\text{des}}) \in [0, H]$, *currently* perceived along direction α_{des}:

$$v_{\text{des}}(t) = \min\left(v_{\text{opt}}, \frac{D\left(\alpha_{\text{des}}\right)}{\tau_1}\right)\ . \tag{2}$$

The actual velocity vector $\vec{v}(t)$ is continuously adjusted depending on $\vec{v}_{\text{des}}(t)$:

$$\frac{d\vec{v}}{dt} = \frac{\vec{v}_{\text{des}}(t) - \vec{v}(t)}{\tau_2}\,, \tag{3}$$

where the fixed parameter τ_2 represents the *time constant* characterizing the exponential speed profile, which in practice modulates the smoothness of motion. From controlled laboratory experiments for pedestrians in normal walking conditions it has been observed that $\tau_1 = \tau_2 = 0.5$ s [21].

Note that, since computing $f(\alpha)$ values involves a rough prediction of agent's and obstacles' future trajectories, the resulting behavior is *proactive* in that it attempts to avoid potential collisions well before they are expected to occur.

3.2 Implementation of the Model for Robotic Agents

The model described above results in smooth paths, which have shown to closely match the characteristics of pedestrian motion in large-scale controlled experiments, both for single trajectories and macroscopic crowd motion patterns [19]. Robots following the same rules, and with human-like sensing and locomotion ability, are therefore expected to exhibit the same large-scale, macroscopic behaviors observed in human crowds. They would also exhibit behaviors which are predictable (and thus acceptable) by humans sharing the same environment.

Unfortunately, the presented heuristic does not ensure collision-free behavior: in fact, small collisions (e.g., shoulder to shoulder) among humans happen frequently and contribute to shape the behavior of tightly-packed crowds. However, collisions are not really acceptable in robotics. The problem is further aggravated by inaccuracies in localizing other agents (especially when using low resolution cameras, as typical in swarm systems). Therefore, we introduce a system parameter *safety margin* m_s, defined by augmenting the radius of all obstacles, to be accounted for during the computation of the $f(\alpha)$ function (in the experiments we set $m_s = 0.1$ m).

Through an experimental study we investigate the small-scale (Section 5.2) and macroscopic (Sections 5.3 and 5.4) properties of the robot navigation algorithm as described above. In the next section we discuss a specific enhancement of the model which promotes the emergence of interesting macroscopic behaviors in robot swarms, which is experimentally tested in Section 5.5.

3.3 Enhancements for Socially Active Robots

We consider the setting in which the robots in the swarm belong to *different classes*. Such classes may represent different types of robots, possibly with different locomotion characteristics and navigation attitudes. However, even in a swarm composed by physically homogeneous robots, different classes may represent other types of relations, such as different roles or responsibilities in the swarm, or different levels of behavioral affinities among groups (e.g., elderly vs. youngsters). In this context we investigate a bio-inspired approach for promoting

the autonomous emergence of grouping behaviors among the robots in the same class.

To each agent a we associate an internal, time-variant state $w_a \in \mathbb{R}$ – an adimensional quantity which we refer to as *wellness*. The wellness of an agent represents its *emotional state* in relation to the navigation and the presence of agents of the same or different groups. The perception of wellness modulates the obstacle-avoidance behavior of an agents, and depends on how well, in terms of class membership, the robot fits within its neighborhood. Let us define

$$\theta(a,b) = \begin{cases} +1 & \text{if } a \text{ and } b \text{ belong to the same class} \\ -1 & \text{otherwise} \end{cases} \tag{4}$$

then, w_a is computed as:

$$w_a = \sum_{b \in \text{visible neighbors}} \theta(a,b)\ e^{-\frac{d(a,b)}{g}}\,, \tag{5}$$

where $d(a,b)$ denotes the distance between the agents a and b, and g defines the spatial scale of the influence of the neighbors on the agent's wellness.

An agent with a large w_a value *feels* well and safe, since most of its closest visible neighbors belong to its own class. On the contrary, agents whose closest visible neighbors belong to a different class are associated to negative wellness values. A lonely agent feels neutral ($w_a = 0$). w_a may alter different aspects of the agent's sensing and/or behavior as to mimic human brain neuromodulation [13]. In the following, we let w_a modulate the agent's optimal speed (v_{opt} in Eq. (2)) such that a robot, when it does not feels safe, will tend to be more cautious and move slower. In Eq. (2), we replace v_{opt} with $v_{\text{opt}} - \Delta(w_a)$. $\Delta(w_a)$ is defined as follows:

$$\Delta(w_a) = \begin{cases} 0 & \text{if } w_a \geq 0\,, \\ \Delta_{\max} & \text{if } -kw_a > \Delta_{\max}\,, \\ -kw_a & \text{otherwise}\,, \end{cases} \tag{6}$$

where $\Delta_{\max} \geq 0$ (measured in m/s) is a parameter bounding the maximum effect of wellness on the optimal speed, and $k \geq 0$ (also measured in m/s) is a parameter controlling how much effect the agent's wellness has on its own speed.

Section 5.5 shows that this modeling results in robots of the same class clustering together, led by cautious group leaders.

4 Implementation on Real and Simulated Robots

The navigation algorithm described in Section 3 has been implemented on real robots (the *foot-bots*) as well as in simulations.

4.1 The foot-bot real robot platform

The *foot-bot* robot is a small mobile platform, directly derived from the *marXbot* [2], specifically designed for swarm robotics [22]. The robot is 17 cm wide and 30 cm tall, and is based on an on-board ARM-11 processor programmed in a Linux-based operating environment. Differential-driven motorized tracks allow mobility at speeds up to 0.3 m/s.

In the context of this work, foot-bots sense neighbors by means of a forward-facing camera with a $2\phi = 50°$ field of view and a down-sampled resolution of 128×92 px, which is used for localizing humans, navigation targets, and walls at 25 frames-per-second.

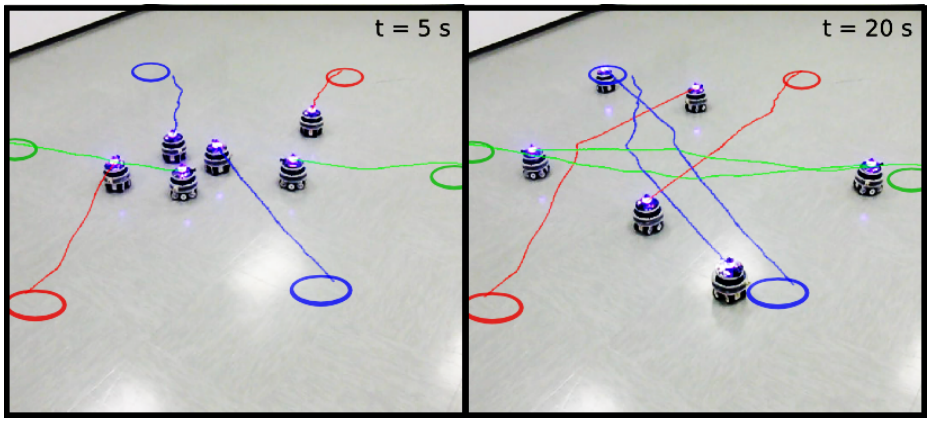

Fig. 2. Six *foot-bot* robots implementing our algorithms, moving towards opposite sides of a circle without collisions. Full video at `http://bit.ly/WkJOld`

Since our main focus is on navigation algorithms and not on sensing, we use straightforward techniques for processing camera images: entities of interest, (e.g., landmarks used to identify a destination point, or humans) are marked with differently colored bands at a known height from the floor. Robots convert each frame to the HSV color space, and segment pixels corresponding to each object. After performing connected component analysis, this results in a set of binary blobs. From the image coordinates of each blob's centroid, the robot computes distance and bearing of the corresponding entity by means of an homography transform, which can be estimated in advance given that the camera parameters and height of each entity are known. The velocity of humans is estimated by finite differencing, after smoothing position readings with a moving average filter defined over a period of 0.5 s. Note that the position of targets (i.e., destination points) is sensed online through vision, and not given by an external observer or a higher-level path planning algorithm.

Robot controllers operate on a 0.1 s timestep and are not synchronized with each other. At each timestep, rules in Eq. (1) and (2) yield the desired values

for heading (α_{des}) and speed (v_{des}), respectively. Both in simulation and in the implementation on the foot-bots, we use a mobility model similar to Eq. (3) that takes into account the robots constraints and independently controls the speed of the two differential driven track wheels.

4.2 Robot simulation

We developed a custom simulator for the efficient and accurate simulation of large foot-bot swarms. In the simulation experiments, the observed position and speed of neighboring agents (i.e., the readings of simulated sensors) are artificially corrupted by random localization errors approximating the statistical properties of errors observed in the real implementation. This means a precise and uniform bearing resolution but large uncertainty in depth estimation, which increases for objects farther away. More specifically, given an obstacle whose ground truth relative position is expressed in robot-centered polar coordinates as (ρ, θ), the observed position (ρ', θ') is given by $(\theta' = \theta + \phi e;\ \rho' = \rho + \gamma\rho\phi e)$. In the formulae, $e \sim \mathcal{N}(0, \sigma)$ models the localization error in the normalized image space, ϕ denotes the camera field of view, and γ is a constant depending on the characteristics of the depth estimation approach. In the following, we set $\sigma = 1/128$ (i.e., 1 pixel on a 128×96 sensor) and $\gamma = 10$. In both the real and simulated robot implementations, velocity vectors are estimated by finite differencing.

5 Experimental Results

In this section, we report the results of experiments aimed at studying the effect of the proposed algorithm in terms of: (i) efficiency of individual trajectories (Section 5.2), and (ii) emergence of macroscopic behavioral patterns (Sections 5.3, 5.4 and 5.5). These aspects are investigated in two different experimental settings, denoted as *cross* and *periodic corridor*, respectively.

In the *cross* setting, we consider four target destinations at the vertices of a square with an edge of 4 m. N robots are divided in two equally-sized groups: robots of each group travel back and forth between two opposite vertices, thus creating a busy crossroad in the middle (see Figure 3). In this setting, we use infrared range and bearing sensors for robot-robot detection both in real robot implementation and in simulation. In the *periodic corridor* setting, $N = 60$ robots travel along a straight corridor with a given width w_C and fixed length $l_C = 16m$, whose opposite ends "wrap around" as if the corridor was the lateral surface of a cylinder. This setting is often considered in the crowd analysis literature, and allows us to observe emerging macroscopic behaviors.

For each experiment we study the effects of one or two parameters. For each setting of the parameters we perform 100 simulation runs (replicas), each lasting 360 s of simulated time. For each run, robots are positioned in randomly chosen initial locations.

5.1 Performance Metrics

We define several metrics, for quantifying the quality of individual trajectories (*relative throughput* and *path irregularity*), and for observing the emergence of macroscopic behaviors in the *periodic corridor* scenario (*line order*, *group order*, and *number of clusters*).

Trajectory quality metrics

Relative throughput is defined as the number of targets that a robot has reached during the simulation, expressed as a fraction of the number of targets that the robot could reach if traveling along straight paths and ignoring collisions (which is an ideal upper bound for throughput). The measure is adimensional and is averaged over all the robots in the simulation.

Path irregularity is defined as the amount of *unnecessary turning* per unit path length performed by a robot, where *unnecessary turning* corresponds to the total amount of robot rotation minus the minimum amount of rotation which would be needed to reach the same targets with the most direct path. Path irregularity is measured in rad/m, and is averaged over all the robots in the simulation.

Macroscopic order metrics

For the *periodic corridor* scenario, following [1], we extend the approach in [23] and define three macroscopic order metrics quantifying interesting characteristics of the agents' spatial configuration at a given moment in time.

Let $\mathcal{L}$ denote the set of all longitudinal corridor bands with width Δ_L and spanning the entire length of the corridor. Let $L(x) = [x, x + \Delta_L] \times [0, l_C] \in \mathcal{L}$ denote one specific band. Similarly, let $\mathcal{T}$ denote the set of all transversal corridor bands with length Δ_T, and let $T(y) = [0, w_C] \times [y, y + \Delta_T] \in \mathcal{T}$ denote one specific band.

Let $n_k(B)$ be the number of agents of class k whose center lies inside a transversal or longitudinal band $B \in \mathcal{L} \cup \mathcal{T}$. In the 2-class case, the Yamori's band index $Y(B)$ [23] measures the prevalence of any class in B, and is defined as:

$$Y(B) = \frac{|n_1(B) - n_2(B)|}{n_1(B) + n_2(B)}$$

Line order: the line order O_L is defined as the average Yamori index of longitudinal bands of width $\Delta_L = 0.3$ m over $\mathcal{L}$, and measures how agents of the same class tend to position themselves along ordered longitudinal lines. O_L is bounded between 0 (random configuration) and 1 (representing perfect organization of the swarm classes in longitudinal lines).

$$O_L = \langle Y(B) \rangle_{B \in \mathcal{L}}$$

Group order: the group order O_G is defined as the average Yamori index of transversal bands of length $\Delta_T = 0.6$ m over $\mathcal{T}$, and quantifies how agents of the same class tend to group themselves in compact clusters. $0 \leq O_G \leq 1$, with $O_G = 1$ meaning perfect organization of the swarm classes in clusters.

$$O_G = \langle Y(B) \rangle_{B \in \mathcal{T}}$$

Number of clusters: the number of clusters N_G is computed as follows. Let $\{T_1, T_2\}$ denote a pair of adjacent transversal bands of length $\Delta_T = 0.6$ m. N_G is defined as the number of such pairs where the majority class in T_1 differs from the majority class in T_2.

5.2 Algorithm Scalability and Trajectory Efficiency

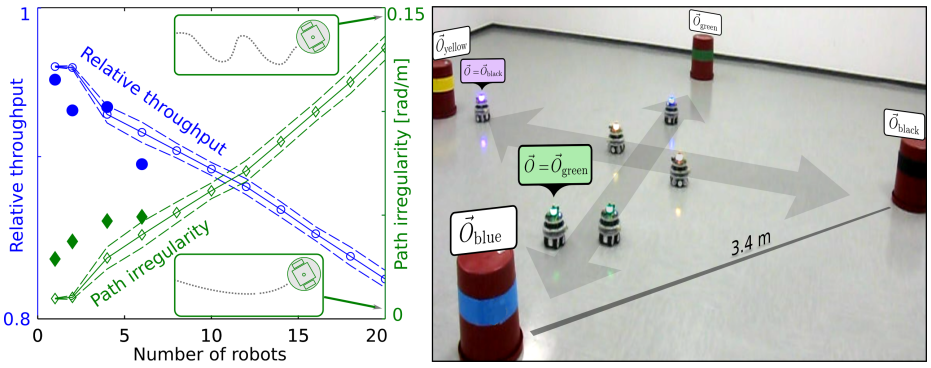

Fig. 3. Experimental results (left) for scalability in the *cross* scenario (pictured on the right). Large filled markers correspond to results measured on real robots. Blue thick line with round markers denotes relative throughput. Green thin line with diamond markers shows path irregularity. Dashed lines delimit ± standard deviation over 100 randomly initialized replicas. In this experiment, both real and simulated robots use 360° range-and-bearing sensing, $H = 3$ m, $m_s = 10$ cm.

Within scenario *cross*, we initially verify the scalability of the algorithm versus an increasing number of agents, and validate simulation results by comparison with the performance measured on foot-bot robots. Results are reported in Figure 3. We can observe that the results obtained with real robots in the same conditions closely match simulations. As the swarm size grows, relative throughput decreases and path irregularity increases, because robots must follow longer and more curvy trajectories in order to avoid collisions. Performance scales well, since, even in very dense scenarios, paths remain efficient, smooth, and predictable.

In the real robot implementation, despite the severe hardware limitations, the navigation controller requires invariably less than 20 ms of computation time per

timestep. In simulation, we also tested robustness to timesteps longer than 0.1 s, and found that in all considered scenarios, performance begins to degrade only when the timestep exceeds 0.4 s.

5.3 Formation of Ordered Lines of Opposite Flow

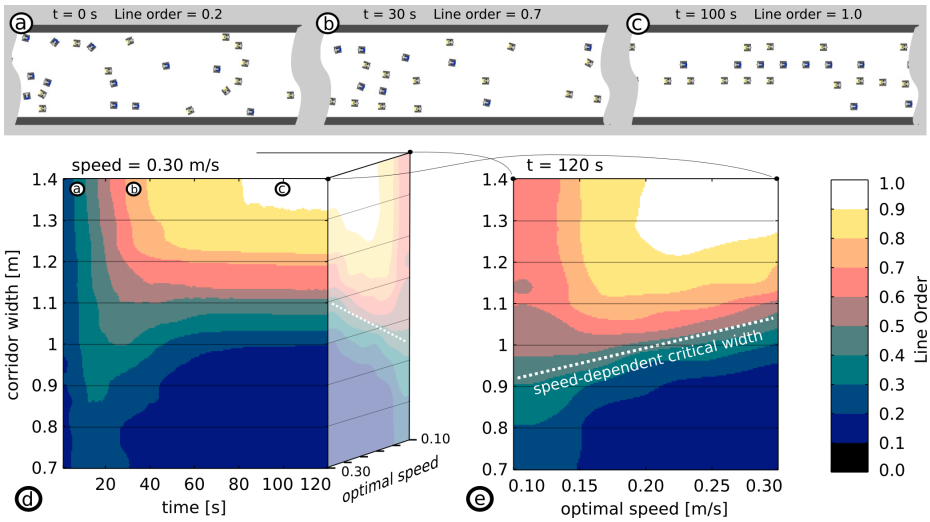

Fig. 4. Formation of flow lines when the corridor is shared by 60 robots traveling in different directions (30 dark blue: to the left; 30 bright yellow: to the right). ⓐ, ⓑ, ⓒ: configuration at $t = \{0, 30, 100\}$ s. ⓓ: line order (color value) as function of time (x axis) and corridor width (y axis), for robot speed $v_{\text{opt}} = 0.3$ m/s. Datapoints corresponding to configurations a,b,c are marked. ⓔ: line order at $t = 120$ s, as function of v_{opt} (x axis) and corridor width (y axis).

For the remaining experiments, we consider the *periodic corridor* scenario.We observe that robots traveling in opposite directions, just like pedestrians, tend to form stable ordered lines of flow from initial random settings. This macroscopic collective behavior results in increased efficiency, since agents can follow more direct trajectories. In Figure 4 we illustrate this process, and show that there is a critical corridor width below which robots are too dense to reach an ordered formation. Such critical density is also influenced by robot parameters. Figure 4ⓔ shows that the critical width depends on the value of v_{opt}: faster robots need larger maneuvering spaces, and therefore require a larger corridor for reaching an ordered configuration.

5.4 Effects of Sensing On Line Order

In Figure 5 we study how the sensing methodology used for localizing neighbors affects swarm's macroscopic behaviors. Unlike humans, which exhibit very little

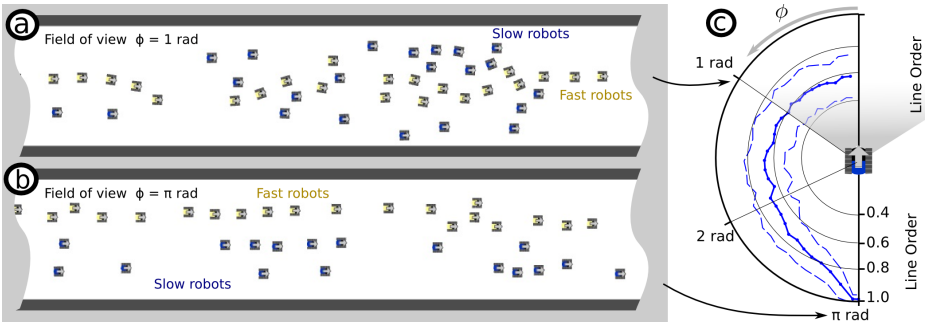

Fig. 5. 30 slow (dark blue) and 30 fast (bright yellow) robots sharing the corridor (w_c=2 m) traveling in the same direction (right), for different values of the half-field of view ϕ of slow robots. ⓐ, ⓑ: configuration at $t = 300$ s, for $\phi = 1$ rad and $\phi = \pi$ rad, respectively. ⓒ: line order at $t = 300$ s as a function of ϕ. Dashed lines represent ± 1 standard deviations over 100 replicas.

variations in their ability to sense the environment, different types of robots may feature very different sensing subsystems. We consider the case in which two types of robots – *fast* and *slow* – move along the corridor in the same direction, with different speeds, equal to 0.1 m/s and 0.3 m/s. We study how the field of view ϕ of the slow robots affects the ability to reach an ordered configuration.

With low ϕ values, slow robots cannot perceive and react to fast robots approaching behind them. In contrast, fast robots frequently need to steer around slow ones. As a consequence, fast robots tend to form ordered but zigzagging line-like structures, whereas slower robots remain scattered because they rarely need to navigate around obstacles.

On the contrary, when slow robots are able to perceive neighbors in a large field of view (e.g., by using omnidirectional cameras or additional back-pointing sensors), both robot types reach a well-ordered configuration. In fact, slow robots are now able to anticipate that they are being overtaken, and steer accordingly. This enables the formation of flow lines for both groups, therefore resulting in a very efficient configuration.

5.5 Emergence of Homogeneous Groups with Socially Active Robots

Figure 6 illustrates how the socially-active, emotion-driven behavior model described in Section 3.3 leads to the emergence of collective grouping behaviors. Two classes of robots are considered. They are identical in terms of mobility and travel along the corridor in the same direction. After a short time, the robots cluster in a limited number of class-homogeneous groups, led by cautions agents with low wellness values: such agents only perceive neighbors of a different class.

We study how group order improves with time while robots cluster in fewer, larger groups. When the wellness-induced speed modulation k is large, robots quickly reach an ordered setting, whereas they require a much longer time for small k. We also show how the g parameter, which defines the influence radius

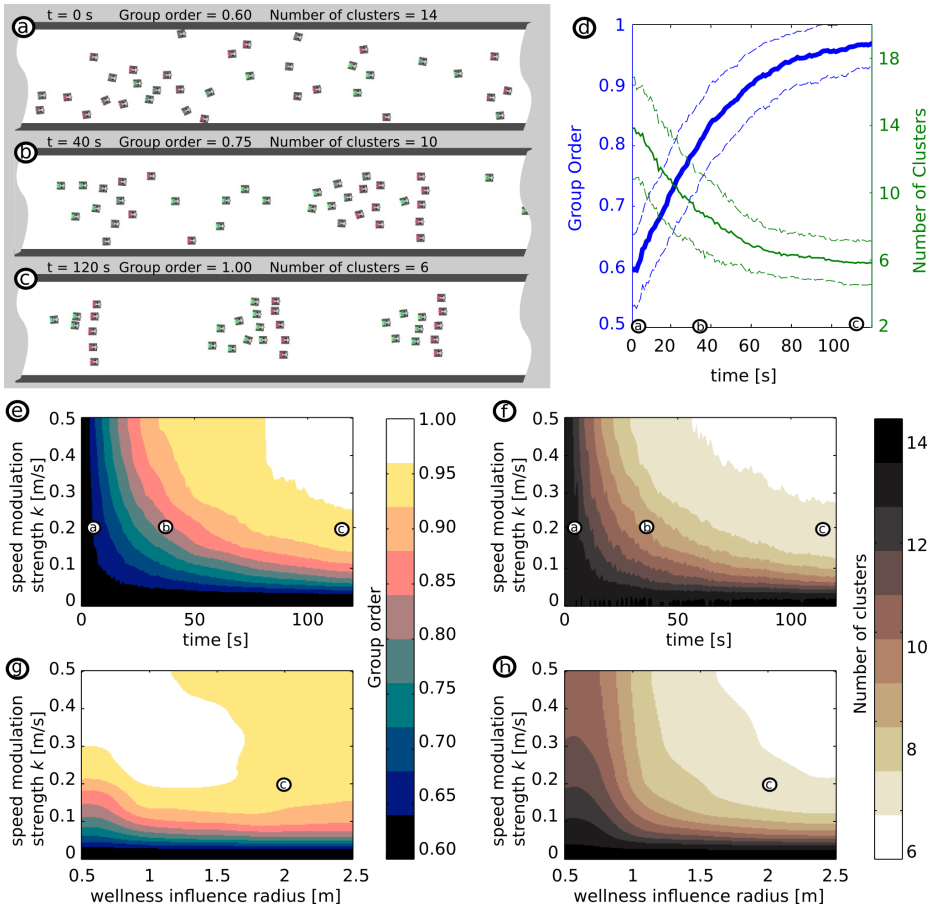

Fig. 6. Two classes of 30 robots (with wellness-controlled speed) sharing the corridor (width $w_C = 2$ m), traveling in the same direction (right). ⓐ, ⓑ, ⓒ: configuration at $t = \{0, 40, 120\}$ s, with $g = 2$ m, $k = 0.2$ m; robot colors are mapped to their wellness value w_a (dark red: low; bright green: high); note formation of groups led by cautious robots with low w_a. ⓓ: group order (thick blue line) and number of clusters (thin green line) against time (x axis). ⓔ: group order (color value) against time (x axis) and value of speed modulation strength k (y axis), with $g = 2$ m. ⓕ: number of clusters in the same context. ⓖ: group order (color value) against g (x axis) and k (y axis) at $t = 120$ s. ⓗ: number of clusters in the same context.

of neighbors on an agent's wellness, has little effect on the speed of the process, but it affects the number (and size) of the resulting groups. In particular, when g is large, robots tend to cluster in a few, large groups. Otherwise, stable configurations with several small groups emerge.

6 Conclusions

We introduced a novel obstacle avoidance algorithm for robot swarms based on a heuristic that closely models the behavior of human pedestrians. We have presented an implementation on real robots as well as on a simulator capable to handle several different scenarios of interest. We studied the characteristics and the efficiency of the obtained navigation trajectories in a number of extensive simulation tests (validated by real robot tests).

We observed that robot swarms implementing our algorithm exhibit several macroscopic behaviors which can also be observed in human crowds, such as the formation of ordered lines of flow in corridors. We investigated how different environment properties or algorithm parameters affect such emergent behaviors, and introduced a simple neuro-modulation/emotional model which promotes the emergence of new behaviors, such as the ability to form groups in heterogeneous swarms.

We are currently advancing the implementation on real robots in order to test the system in scenarios in which the space is shared between humans and robots, and/or among robots with very different mobility characteristics. Moreover, we are running simulations comparing our approach with state-of-the art obstacle avoidance algorithms. In addition, we are designing experiments for quantitatively evaluating our main objective, i.e. the predictability and perceived friendliness of robots' trajectories by humans.

References

1. Mehdi Moussaïd, Dirk Helbing, and Guy Theraulaz. How simple rules determine pedestrian behavior and crowd disasters. *Proceedings of the National Academy of Sciences of the United States of America*, 108(17):6884–8, 2011.
2. M. Bonani, V. Longchamp, S. Magnenat, P. Rétornaz, D. Burnier, G. Roulet, F. Vaussard, H. Bleuler, and F. Mondada. The marXbot, a miniature mobile robot opening new perspectives for the collective-robotic research. In *Proc. of the IEEE/RSJ International Conference on Intelligent Robots and Systems (IROS)*, pages 4187–4193, 2010.
3. Zvi Shillert and P. Fiorini. Motion planning in dynamic environments using velocity obstacles. *The International Journal of Robotics Research*, 17(7):760–772, 1998.
4. Boris Kluge and E Prassler. Recursive agent modeling with probabilistic velocity obstacles for mobile robot navigation among humans. In *Proceedings IEEE/RSJ International Conference on Intelligent Robots and Systems*, volume 1, pages 376–381, 2003.
5. Jur van den Berg, Dinesh Manocha, and Ming Lin. Reciprocal velocity obstacles for real-time multi-agent navigation. In *Proceedings of IEEE International Conference on Robotics and Automation*, pages 1928–1935, 2008.
6. Jamie Snape, Jur van den Berg, Stephen J. Guy, and Dinesh Manocha. The hybrid reciprocal velocity obstacle. *IEEE Transactions on Robotics*, 27(4):696–706, 2011.
7. Stephen J. Guy, Ming C. Lin, and Dinesh Manocha. Modeling collision avoidance behavior for virtual humans. In *Proceedings of the International Conference on Autonomous Agents and Multiagent Systems*, pages 575–582, 2010.

8. J. J. Gibson. Visually controlled locomotion and visual orientation in animals. *British journal of psychology*, 49(3):182–194, 1958.
9. Matthieu François, Antoine H. Morice, Reinoud J. Bootsma, and Gilles Montagne. Visual control of walking velocity. *Neuroscience research*, 70(2):214–9, 2011.
10. Reinoud J Bootsma and Cathy M Craig. Information used in detecting upcoming collision. *Perception*, 32(5):525–44, 2003.
11. D. N. Lee. A theory of visual control of braking based on information about time-to-collision. *Perception*, 5(4):437–59, 1976.
12. Jennifer T. Coull, Franck Vidal, Ceydric Goulon, Bruno Nazarian, and Cathy Craig. Using time-to-contact information to assess potential collision modulates both visual and temporal prediction networks. *Frontiers in human neuroscience*, 2(September):10, 2008.
13. J. L. Krichmar. The neuromodulatory system: a framework for survival and adaptive behavior in a challenging world. *Adaptive Behavior*, 16(6):385–399, 2008.
14. Brian R. Cox and Jeffrey L. Krichmar. Neuromodulation as a robot controller: a brain inspired strategy for controlling autonomous robots. *IEEE Robotics & Automation Magazine*, 16(3):1–25, September 2009.
15. Jeffrey L. Krichmar. A biologically inspired action selection algorithm based on principles of neuromodulation. In *Proceedings of IEEE World Congress on Computational Intelligence*, pages 10–15, 2012.
16. Edward T Hall. A system for the notation of proxemic behavior. *American Anthropologist*, 65(5):1003–1026, 1963.
17. D. Helbing, I. Farkas, and T. Vicsek. Simulating dynamical features of escape panic. *Nature*, 407(6803):487–490, 2000.
18. Anders Johansson. Constant-net-time headway as key mechanism behind pedestrian flow dynamics. *Physical Review E*, 80:026120, 2009.
19. Mehdi Moussaïd, Elsa G. Guillot, Mathieu Moreau, Jérôme Fehrenbach, Olivier Chabiron, Samuel Lemercier, Julien Pettré, Cécile Appert-Rolland, Pierre Degond, and Guy Theraulaz. Traffic instabilities in self-organized pedestrian crowds. *PLoS computational biology*, 8(3):e1002442, 2012.
20. Dirk Helbing, Péter Molnár, Illés J. Farkas, and Kai Bolay. Self-organizing pedestrian movement. *Environment and Planning B: Planning and Design*, 28(3):361–383, 2001.
21. Mehdi Moussaïd, Dirk Helbing, Simon Garnier, Anders Johansson, Maud Combe, and Guy Theraulaz. Experimental study of the behavioural mechanisms underlying self-organization in human crowds. *Proceedings of the Royal Society B*, 276(1668):2755–2762, 2009.
22. M. Dorigo, D. Floreano, L. M. Gambardella, F. Mondada, S. Nolfi, T. Baaboura, M. Birattari, M. Bonani, M. Brambilla, A. Brutschy, D. Burnier, A. Campo, A. L. Christensen, A. Decugnière, G. A. Di Caro, F. Ducatelle, E. Ferrante, A. Förster, J. Martinez Gonzales, J. Guzzi, V. Longchamp, S. Magnenat, N. Mathews, M. Montes de Oca, R. O'Grady, C. Pinciroli, G. Pini, P. Rétornaz, J. Roberts, V. Sperati, T. Stirling, A. Stranieri, T. Stützle, V. Trianni, E. Tuci, A. E. Turgut, and F. Vaussard. Swarmanoid: a novel concept for the study of heterogeneous robotic swarms. *IEEE Robotics & Automation Magazine*, 2012 (to appear).
23. Katsuya Yamori. Going with the flow: Micro–macro dynamics in the macrobehavioral patterns of pedestrian crowds. *Psychological review*, 105(3):530–557, 1998.